

Oligomeric Acceptor Enables High-Performance and Robust All-Polymer Solar Cells with 17.4% Efficiency

Zhixiang Li, Zhe Zhang, Hongbin Chen, Yunxin Zhang, Yuan-Qiu-Qiang Yi, Ziqi Liang, Bin Zhao, Miaomiao Li, Chenxi Li, Zhaoyang Yao, Xiangjian Wan, Bin Kan,* and Yongsheng Chen*

Developing efficient and stable all-polymer solar cells (all-PSCs) has received increasing attention because of their mechanical robustness for flexible devices. Based on the CH-series small molecule acceptors, a new polymer acceptor (PZC24) is reported and obtains a decent power conversion efficiency (PCE) of 16.82% when blended with PM6. To further improve the performance, an oligomeric acceptor (CH-D1), which possesses the same backbone structure as PZC24, is proposed and synthesized as the third component for all-PSC system. The creative strategy improves the crystallinity and molecular packing, and can maintain the efficient charge transport channels of the all-PSCs binary system. Therefore, the PM6:PZC24:CH-D1 based ternary devices exhibit an impressive PCE of 17.40%, among the highest value of all-PSCs. Compared to the PM6:PZC24, the ternary device exhibits enhanced photo-soaking stability and thermal stability, simultaneously. In addition, the introduction of oligomeric acceptor does not weaken the mechanical robustness of all-PSCs. As such, the ternary flexible devices display an excellent PCE of 15.35%. Importantly, this strategy shows excellent universality in PM6:PY-IT and PM6:PY-V- γ all-PSCs with improved PCEs over 17%. The results provide a feasible strategy to simultaneously improve photovoltaic efficiency and stability of all-PSCs devices and herald a bright future for all-PSCs.

1. Introduction

Organic solar cells (OSCs) have attracted considerable attention due to their unique features, such as light weight, flexibility, semitransparency, and feasibility in wearable electronics.^[1–4] In recent years, thanks to the innovation of the photovoltaic materials, interface engineering and the morphology modulation of active layer, the power conversion efficiencies (PCEs) of single-junction OSCs based on polymer donors: small molecule acceptors (SMAs) have exceeded 19%.^[5–21] Among various systems of OSCs, all-polymer solar cells (all-PSCs), which contain both polymer donors (P_{Ds}) and polymer acceptors (P_{As}) in the active layer, possess great potential for practical applications due to the remarkable merits such as superior stability, mechanical flexibility, and stress robustness.^[22–28] However, quite few all-PSCs can afford impressive PCEs of over 17%, which lag far behind those of SMAs-based OSCs.^[22–24,26,29–37] The main reasons are the lower extinction coefficient versus

Z. Li, Z. Zhang, H. Chen, C. Li, Z. Yao, X. Wan, Y. Chen
State Key Laboratory and Institute of Elemento-Organic Chemistry
The Centre of Nanoscale Science and Technology and Key Laboratory
of Functional Polymer Materials
Renewable Energy Conversion and Storage Center (RECAST)
College of Chemistry
Nankai University
Tianjin 300071, China
E-mail: yschen99@nankai.edu.cn
Y. Zhang, B. Kan
School of Materials Science and Engineering
National Institute for Advanced Materials
Nankai University
Tianjin 300350, China
E-mail: kanbin04@nankai.edu.cn

Y.-Q.-Q. Yi
Printable Electronics Research Center
Nano Devices and Materials Division
Suzhou Institute of Nano-Tech and Nano-Bionics
Chinese Academy of Sciences
Suzhou, Jiangsu 215123, China
Z. Liang, B. Zhao, M. Li
School of Materials Science and Engineering, and Tianjin Key
Laboratory of Molecular Optoelectronic Science
Tianjin University
Tianjin 300072, China

 The ORCID identification number(s) for the author(s) of this article can be found under <https://doi.org/10.1002/aenm.202300301>.

DOI: 10.1002/aenm.202300301

that of SMAs limits the short-circuit current densities (J_{SCs}), and the unfavorable morphology caused by large conjugated lengths and high molecular weights of P_A and P_D materials tends to suppress the fill factors (FFs).^[38–42]

To solve these issues, “polymerized small molecule acceptor” (PSMA) strategy,^[43,44] ternary strategy,^[45] and device engineering^[30,31,33,46] are considered as efficient approaches to be developed continually. Among various device optimization methods, fabricating the ternary blends has been proved as an advantageous and simple strategy to uplift device performance. It is worth noting that the third component plays an important role in enhancing light absorption, facilitating charge transfer, and optimizing nanoscale morphology in the ternary systems.^[34,47] In previous work on all-PSCs, the third components could be P_{DS} , P_{AS} , or small molecule acceptors.^[26,29,34,48,49] For example, the strategy of choosing a similar P_A to the host one in chemical structure as the third component was reported by Min et al., which improved PCE and stability simultaneously.^[24] Recently, Hou and co-workers introduced PM6 with a high molecular weight into the all-PSCs system to afford efficient pathways for charge transport and mechanical stress dissipation, so that the ternary device demonstrated the PCE of 18.2% with outstanding mechanical properties.^[26] However, because of the difficulty to alter morphology in all-PSCs devices, it is rather challenging to find proper third components, especially a universal one. Recently, Wei et al. reported a “N- π -N” type oligomeric acceptor, which falls in between SMA and P_A and inherited the advantages of both them. Compared to its corresponding SMA, it performed higher tolerance for additive contents, as well as superior stability. While compared to its polymeric counterparts, it could obtain definite molecular structure, increased extinction coefficient, and absence of chains entanglements.^[42] However, the oligomeric acceptors have not been considered to introduce in all-PSCs systems so far.^[40,50–53] Based on this point, it is urgent and significant to study the influence of an oligomeric acceptor as the third component on the performance and mechanical robustness in all-PSCs systems.

With these in mind, we designed and synthesized a polymer acceptor (named PZC24) through linking CH-series SMA^[54–56] by the fluoro-substituted thiophene π bridge. By blending PZC24 with the polymer donor PM6, a decent PCE of 16.82% is achieved. Furthermore, an “N- π -N” type oligomeric acceptor (CH-D1), which has the same core blocks (N type) and linking units (π bridge) as PZC24, was designed and added in PM6:PZC24 system as the third component. Based on the same structure, CH-D1 can be referred as “twins” molecule with PZC24. Therefore, this ternary strategy avoids the complicated selection and additional synthesis for the third component. More importantly, the introduction of CH-D1 leads to stronger crystallinity and more orderly stacking, beneficial from its shorter backbone and less energetic disorder. Compared to their corresponding binary devices, the ternary devices possess more efficient exciton generation rate, exciton dissociation, charge transfer and less charge recombination. Finally, a maximum PCE of 17.40% is recorded in the optimal ternary devices, which outperforms those of the other two corresponding PZC24 and CH-D1 based binary systems (16.82% and 16.62%, respectively), and is among the highest value in the all-PSCs reported so far. Moreover, the ternary devices show superior light-soaking

stability and thermal stability. Impressively, the crack onset strain (COS) is slightly increased by the addition of CH-D1 despite of its lower molecular weight versus P_A . Coupled with that the ternary flexible all-PSCs delivers an outstanding PCE of 15.35%, it demonstrated their great potential for future wearable devices. At the same time, CH-D1 was also introduced to other two typical all-PSCs systems (PM6:PY-IT and PM6:PY-V- γ), in which it obtained similar improvements with high PCEs over 17%, showing the excellent universality of this strategy. Our work not only demonstrates the great potential of oligomeric acceptor as the third component in fabricating high-performance all-PSCs but also provides a feasible strategy to improve photovoltaic efficiency and stability of all-PSCs devices simultaneously.

2. Results and Discussion

2.1. Materials Design and Optical/Electrochemical Properties

The chemical structures of PZC24 and CH-D1 are depicted in **Figure 1**, and their detailed synthesis route is displayed in Scheme S1 in the Supporting Information. The starting material 1 was prepared according to our previous reports.^[54–56] Knoevenagel condensation of compound 1 with 2-(5-bromo-3-oxo-2,3-dihydro-1H-inden-1-ylidene)malononitrile (IC-Br) afforded compound 2 and 3 by controlling the reaction conditions and the ratio of IC-Br. Then, those two compounds proceeded Stille-coupling reaction with 3,4-difluoro-2,5-bis(trimethylstannyl)thiophene to afford polymer acceptor PZC24 and compound 4, respectively. Finally, CH-D1 was acquired from compound 4 through Knoevenagel condensation with 2-(5,6-difluoro-3-oxo-2,3-dihydro-1H-inden-1-ylidene)malononitrile (IC-2F). The detailed synthesis procedures and characterizations including ¹H NMR, ¹³C NMR are provided in the Supporting Information.

The normalized UV–vis absorption spectra of the PZC24 and CH-D1 were investigated and compared in their chloroform (CF) solutions and neat films (Figure 1b; and Figure S1, Supporting Information), and the detail optical characteristics were summarized in **Table 1**. Owing to their same conjugated backbones, the two “twins” acceptors show similar absorption profiles in both solution and film state. As shown in Figure 1b, CH-D1 exhibits a blueshifted absorption compared to PZC24 in their thin-film state, which is consistent with the trend of their solution absorptions in Figure S1a (Supporting Information), and should be due to the preaggregation properties of the polymer. In addition, the film absorption onsets (λ_{onset}) of PZC24 and CH-D1 are 868 and 855 nm corresponding to the optical bandgaps (E_g^{opt}) of 1.43 and 1.45 eV, respectively. The PZC24:CH-D1 blend film prepared from the weight ratio as optimized device of 1:0.3, whose maximized absorption peak lies between those of CH-D1 and PZC24 indubitably, shows the highest absorbance in the intramolecular charge transfer (ICT) region (around 720 nm). The absorption spectra of binary and ternary blends are shown in Figure S1b (Supporting Information), and the λ_{onset} of ternary blend film is similar with that of PM6:PZC24 film (863 nm), indicating the introduction of CH-D1 will not weaken the light-harvesting range in the relevant solar cells.

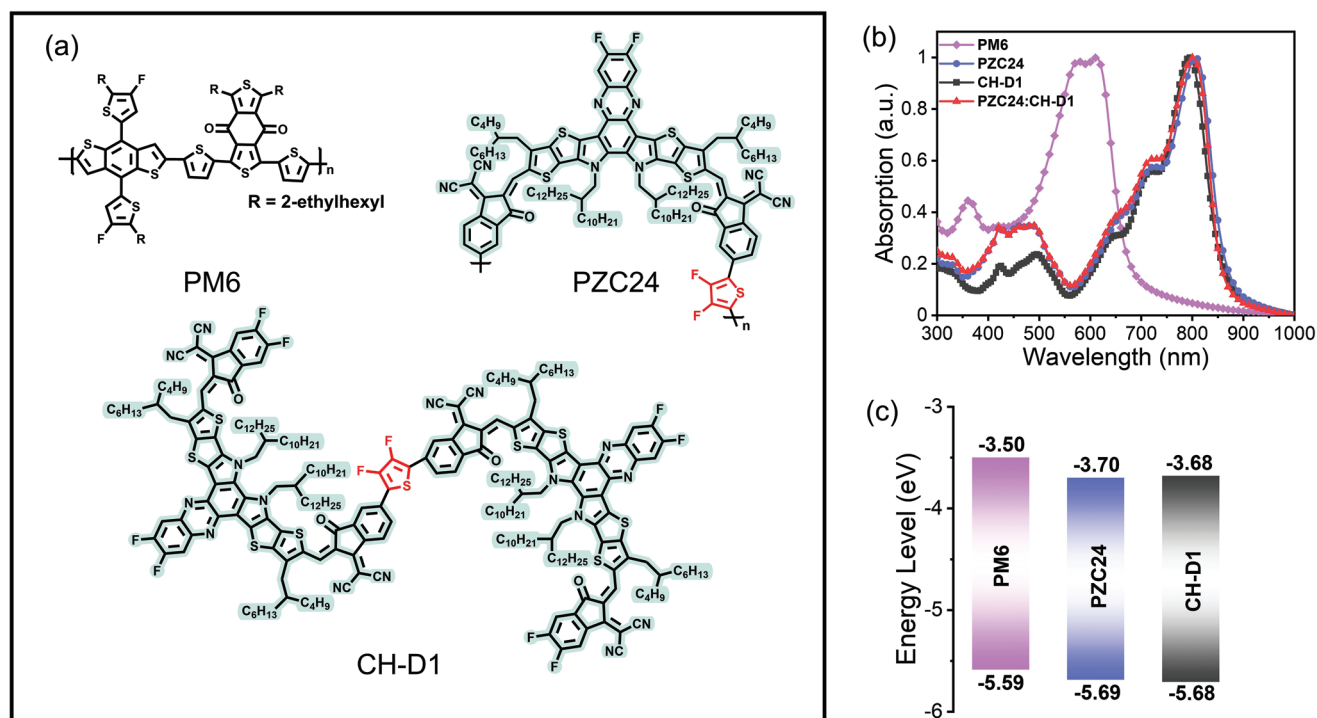


Figure 1. a) Molecular structures of PM6, PZC24 and CH-D1. b) The normalized ultraviolet–visible (UV–vis) absorption spectra in thin films. c) Energy levels diagrams in drop-cast thin films.

The energy levels of the two acceptors as well as polymer donor PM6 were estimated by cyclic voltammetry (CV) (Figure S2, Supporting Information) in the solid state by using ferrocene-ferrocenium (−4.80 eV) standard. As the energy level alignment shown in Figure 1c, both acceptors show well-matched with PM6. Though the highest occupied molecular orbital (HOMO) energy level offsets between PM6 and two acceptors are around 0.10 eV, which are still large enough for the exciton separation in the nonfullerene systems.^[57] In comparison to PZC24, CH-D1 shows slightly lower HOMO (−5.69 to −5.68 eV) but higher lowest unoccupied molecular orbital (LUMO) (−3.68 to −3.70 eV) energy level, resulting in its enhanced electrochemical bandgap, which is consistent with its larger optical bandgap.

2.2. Photovoltaic Properties

To examine effect of a dimer acceptor on the photovoltaic performance, we fabricated all-PSCs with a conventional device configuration of indium tin oxide (ITO)/poly (3,4-ethylenedioxythiophene):poly (styrene-sulfonate) (PEDOT:PSS)/active layer/poly [(9,9-bis(3′-(*N,N*-dimethylamino)propyl)-2,7-fluorene)-alt-5,5′-bis(2,2′-thiophene)-2,6-naphthalene-1,4,5,8-tetracarboxylic-*N,N'*-di(2-ethylhexyl) imide] (PNDIT-F3N)/Ag (Figure 2a) using

PM6 as donor. Detailed experimental procedures are described in the Supporting Information, and optimization data are listed in Tables S1–S6 (Supporting Information). Optimal current density–voltage (*J*–*V*) curves and the corresponding parameters are shown in Figure 2c and Table 2, respectively. The device based on PM6:PZC24 yields a maximum PCE of 16.82% with a high open-circuit voltage (*V*_{OC}) of 0.946 V, an FF of 74.47%, but a moderate *J*_{SC} of 23.76 mA cm^{−2}. In comparison, CH-D1-based device shows a similar *V*_{OC} of 0.949 V although it shows slightly higher LUMO level, a moderate *J*_{SC} of 23.90 mA cm^{−2}, an FF of 73.20%, which all together contribute to a PCE of 16.62%. As can be seen, larger energy loss (*E*_{loss}, defined as *E*_{loss} = *E*_{g,opt} − *eV*_{OC}) limits the performance of CH-D1 based device. Due to the similar structure of PZC24 and CH-D1, we introduced CH-D1 into PM6:PZC24 system to construct ternary blends. The best weight ratio of PM6:PZC24:CH-D1 is optimized to be 1:1:0.3, and the optimized ternary device offers a champion PCE of 17.40% with almost unchanged *V*_{OC} of 0.949 V, a *J*_{SC} of 24.23 mA cm^{−2} and an FF of 75.25%. Notably, the involving of CH-D1 into PM6:PZC24 raises *J*_{SC} and FF simultaneously, which will be discussed in the following. To our knowledge, a PCE of 17.40% is among the highest values to date for all-PSCs devices, showing the feasibility of ternary strategy based on the introduction of dimer acceptor into all-PSCs.

Table 1. The optical and electrochemical properties of PZC24 and CH-D1.

NFAs	$\lambda_{\text{max}}^{\text{CF}}$ [nm]	$\lambda_{\text{max}}^{\text{film}}$ [nm]	$\lambda_{\text{onset}}^{\text{film}}$ [nm]	$E_{\text{g}}^{\text{opt}}$ [eV]	HOMO [eV]	LUMO [eV]
PZC24	789	807	868	1.43	−5.69	−3.70
CH-D1	753	794	855	1.45	−5.68	−3.68

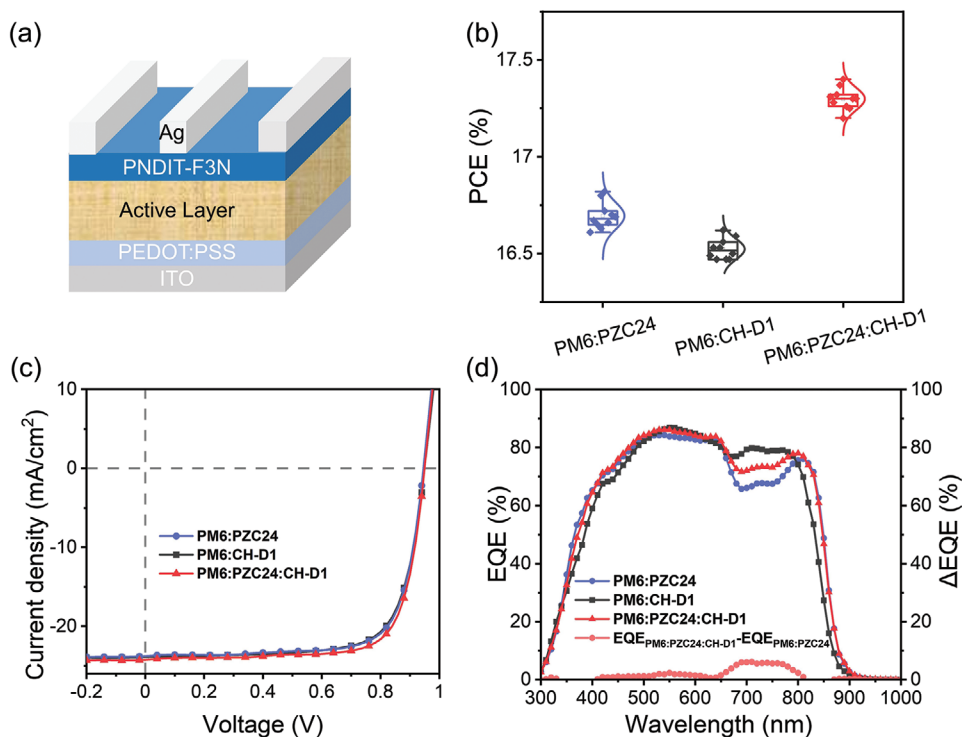


Figure 2. a) Device architecture of OSCs. b) PCE distributions counted by 10 devices. c) J - V curves and d) EQE spectra of OSCs.

Figure 2d displays the external quantum efficiency (EQE) of the devices. The current density integrated from the EQE spectra was 23.28 mA cm^{-2} for PM6:PZC24, 23.32 mA cm^{-2} for PM6:CH-D1, and 23.93 mA cm^{-2} for the ternary system, matching well with the J_{SC} values of the devices from J - V characteristic curves. The PM6:PZC24 blend shows weaker EQE responses throughout the wavelength of acceptor absorption range, in comparison to the PM6:CH-D1 blends. While the narrow EQE response range of CH-D1-based device limits its J_{SC} despite its more efficient photon-electron conversion processes. Combined the advantages of PZC24 with CH-D1, the ternary device generates the highest currents ascribed to a wider absorption wavelength based on PM6:PZC24 system and the enhanced absorbance in the region of 650–800 nm contributed from CH-D1, indicating their higher charge extraction and/or collection efficiencies.

In addition, the long-term device stability is a crucial aspect of OSCs for future practical applications. Therefore, the light-soaking stability and thermal stability at 65°C were examined under the nitrogen atmosphere (Figure S3, Supporting Information). PM6:CH-D1-based device presents better stability under both conditions than all-PSC binary device, especially using light illumination under max power point (MPP) tracking. Therefore, the light-soaking stability evidently increases in ternary all-PSC by introducing CH-D1 to PM6:PZC24 system. Noteworthy, the lifetime of T_{80} (sustained 80% of the initial efficiency) under heat treatment based on PM6:PZC24 and PM6:PZC24:CH-D1 device is measured to be about 320 and 350 h, respectively. The results highlight that the ternary strategy of introducing “twins” dimer acceptor is a promising approach to improve the stability of all-PSC device.

Table 2. Optimized Photovoltaic Parameters of PM6:PZC24, PM6:CH-D1, and PM6:PZC24:CH-D1 systems measured under AM 1.5G.

Active layer	V_{oc} [V]	J_{sc} [mA cm^{-2}]	$J_{\text{sc}}^{\text{EQE}}$ [mA cm^{-2}]	FF [%]	PCE ^{a)} [%]
PM6:PZC24	0.946 (0.945 ± 0.002)	23.76 (23.59 ± 0.16)	23.28	74.47 (74.69 ± 0.28)	16.82 (16.70 ± 0.07)
PM6:CH-D1	0.949 (0.944 ± 0.004)	23.90 (23.72 ± 0.17)	23.32	73.20 (73.56 ± 0.50)	16.62 (16.52 ± 0.05)
PM6: PZC24:CH-D1	0.949 (0.945 ± 0.002)	24.23 (24.41 ± 0.18)	23.93	75.25 (74.90 ± 0.47)	17.40 (17.30 ± 0.05)
PM6: PZC24:CH-D1 ^{b)}	0.939	22.53	21.96	72.60	15.35

^{a)}The average parameters included in the brackets were calculated from 10 devices; ^{b)}Flexible devices.

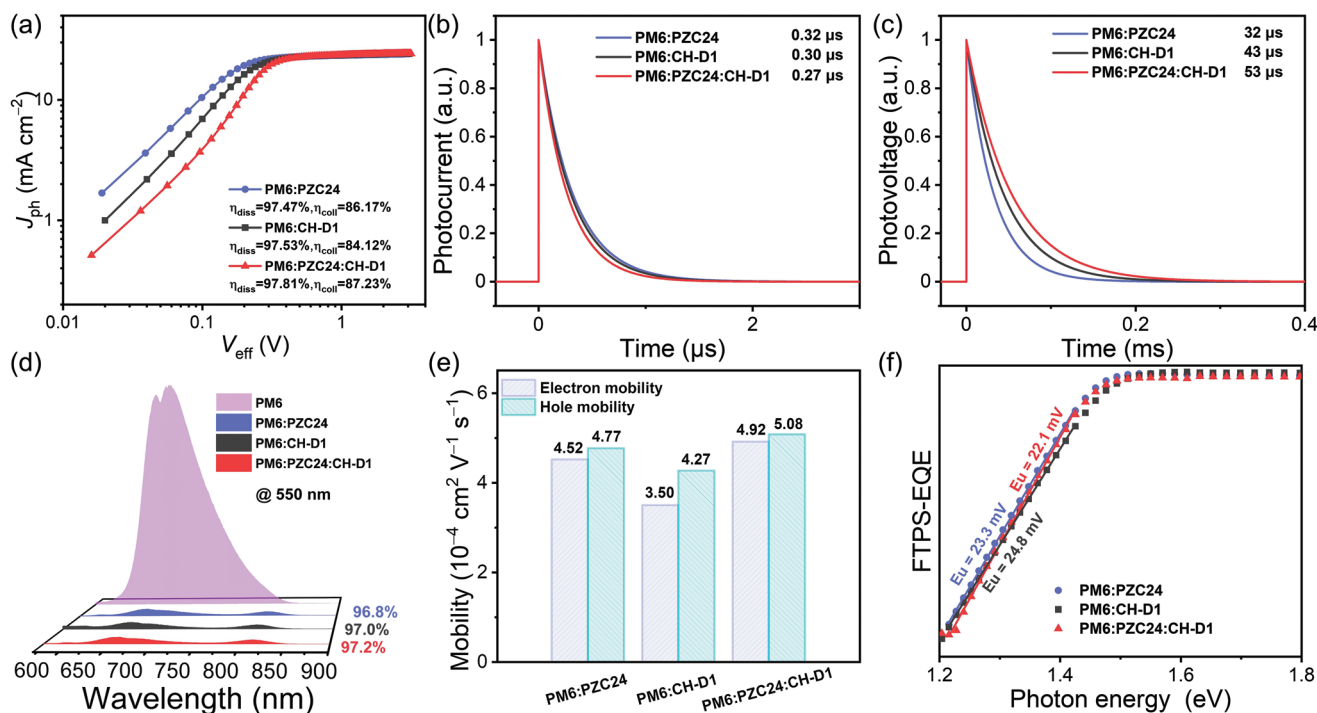


Figure 3. a) J_{ph} - V_{eff} curves. b) Transient photocurrent and c) transient photovoltage measurements of PM6:PZC24, PM6:CH-D1, and PM6:PZC24:CH-D1-based OSCs. d) Photoluminescence (PL) spectra of PM6 neat film and the blend films of PM6:PZC24, PM6:CH-D1, and PM6:PZC24:CH-D1 excited at 550 nm. e) Histograms of the electron mobility (μ_e) and hole mobility (μ_h). f) FTPS-EQEs of PM6:PZC24, PM6:CH-D1, and PM6:PZC24:CH-D1-based OSCs at the absorption onset and their Urbach energy (E_U) values.

2.3. Exciton and Carrier Dynamics

The efficient utilization of the absorbed photons and high FF in ternary systems were convinced by the exciton and carrier dynamics characterization based on the reported methods.^[58–60] First, the plots of the photocurrent density (J_{ph}) versus effective voltage (V_{eff}) are recorded in **Figure 3a**. The exciton dissociation efficiency (η_{diss}) and charge extraction efficiency (η_{coll}) can be assessed from the ratio of J_{ph}/J_{sat} under the short-circuit condition and maximum power output point, respectively, where J_{sat} is defined as J_{ph} reaching saturated state. As results, the ternary device exhibits the highest η_{diss}/η_{coll} (97.81%/87.23%) in comparison with the PM6:PZC24 (97.47%/86.17%) and PM6:CH-D1 (97.53%/84.12%) binary devices, which indicates the efficient exciton dissociation and charge collection behaviors in the PM6:PZC24:CH-D1 ternary device, accounting for the highest EQE response and FF.

Transient photocurrent (TPC) and transient photovoltage (TPV) measurements of the OSCs were further conducted to study the charge recombination characteristic. As plotted in **Figure 3b**, the extraction time of ternary device is extracted to be 0.27 μs , which is the fastest compared to that of PM6:PZC24 (0.32 μs) and PM6:CH-D1 (0.30 μs), implying that the charge extraction is very rapid and less charge is trapped in the ternary device. Additionally, photogenerated carrier lifetime of ternary cell derived from the TPV characterization (**Figure 3c**) is 53 μs , which is much longer than that of PM6:PZC24 (32 μs) and PM6:CH-D1 (43 μs), meaning that charge carrier recombination has been suppressed in the ternary system. The longer

carrier lifetime should be benefitted from the favorable morphology through introducing “twins” oligomeric acceptor in all-PSCs as discussed below.

To study the effect of the dimer acceptor CH-D1 as the third component on charge transport dynamic, steady-state photoluminescence (PL), and space charge-limited current (SCLC) have been measured and illustrated in **Figure 3d,e**, respectively. As can be seen in PL spectra, after blending with PM6, the PM6:PZC24:CH-D1 (1:1:0.3) based film exhibits the most PL quenching efficiency (97.2%) of donor emission, followed by the PM6:PZC24 (97.0%) and PM6:CH-D1 (96.8%) binary films, indicating the effective charge transfer between PM6 and acceptors in the ternary blend. Their hole and electron mobilities (μ_h and μ_e) were evaluated using SCLC method and shown in **Figure 3e**; and **Table S7** (Supporting Information). The binary devices based on PM6:PZC24/PM6:CH-D1 exhibit the hole mobility of 4.77/4.27 $\times 10^{-4}$ and electron mobility of 4.52/3.50 $\times 10^{-4}$ $cm^2 V^{-1} s^{-1}$, respectively. Importantly the ternary cell exhibits the hole and electron mobility of 5.08 $\times 10^{-4}$ and 4.92 $\times 10^{-4}$ $cm^2 V^{-1} s^{-1}$. Compared to the binary blends, the ternary one exhibited the most effective and balanced mobilities, which is beneficial for enhancing charge transport and suppressing charge recombination, respectively, accordingly enhanced J_{SC} and FF.

It has been reported that the Urbach energy (E_U) is described as the width of the tail of the electronic density of states (DOS) for active layers and reflects the degree of overall energy disorder.^[61,62] Thus, the analysis of E_U for different active layers was carried out by fitting the spectra of Fourier-transform

photocurrent spectroscopy EQE (FTPS-EQE). As presented in Figure 3f, the ternary system obtains the smallest E_U with a value of 22.1 mV, compared to that of PM6:PZC24 (23.3 mV) and PM6:CH-D1 (24.8 mV), enabling less trap-assisted recombination of the charge, and much longer charge lifetime, which is agreement with the above results. These results demonstrate that the introduction of “twins” dimer acceptor, CH-D1, is beneficial for all-PSCs to possess more efficient exciton dissociation, less charge carrier recombination, and the higher charge carrier mobility, which guarantees the more efficient charge transport and collection. All these factors contribute the enhanced J_{SC} and FF of the ternary device.

2.4. Morphological Properties

The above-mentioned results drove us to explore the structural characterizations of binary and ternary active layers, which were accomplished by using atomic force microscopy (AFM), grazing incidence wide-angle X-ray diffraction (GIWAXS), and

contact angles measurements. First, as can be seen in AFM height images in Figure 4a–c, PM6:PZC24-based all-PSC forms a more interpenetrating film than that of PM6:CH-D1. Meanwhile, root-mean-square surface roughness (R_q) value of PM6:PZC24 and PM6:CH-D1 films is 0.941 and 1.08 nm, respectively, demonstrating that CH-D1 shows stronger crystalline and molecular assemble ability than polymer PZC24. Surprisingly, when introducing CH-D1 as the third component, the ternary blend film maintains high-quality fibrous structures scatter, which is benefit to charge transport. Besides, the R_q of ternary film (1.07 nm) approaches that of PM6:CH-D1 binary blend, suggesting the strong crystallinity of ternary blend. To make a further corroboration, the fibril widths of the blend films were measured, which is estimated by the full-width at half-maximum of the peaks in the AFM phase images. The line profiles are displayed in Figure S6 (Supporting Information), and the calculated average values are 13.5, 15.6, and 15.1 nm for PM6:PZC24, PM6:CH-D1, and PM6:PZC24:CH-D1 films, respectively. The fiber width of ternary film is quite closed to that of PM6:CH-D1, proving that

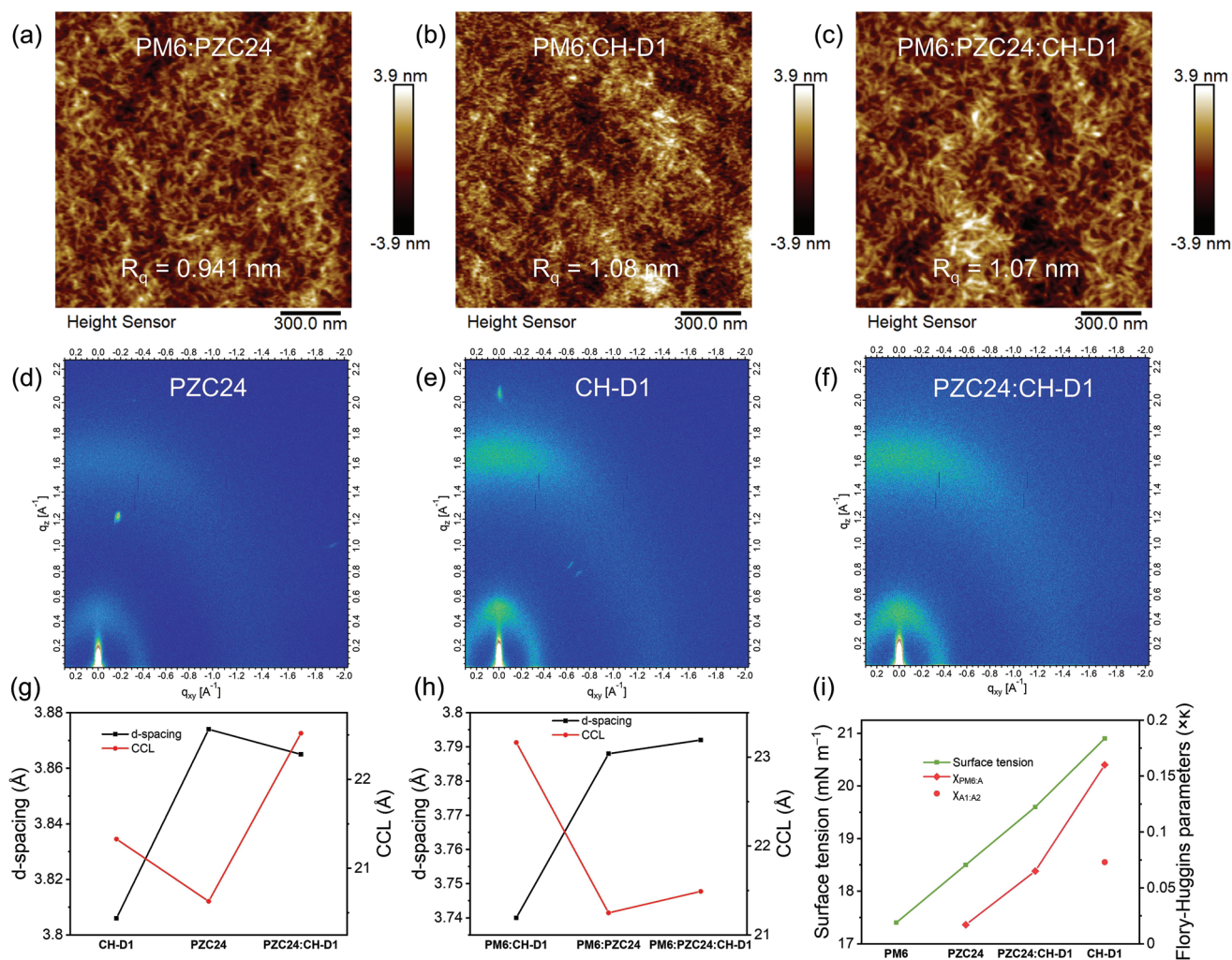


Figure 4. The AFM height images of a) PM6:PZC24, b) PM6:CH-D1, and c) PM6:PZC24:CH-D1 blend films. 2D-GIWAXS patterns of d) PZC24, e) CH-D1, and f) PZC24:CH-D1 (1:0.3, w/w) acceptor films. d-spacing and CCL in π - π stacking direction of g) blend films and h) acceptor films. i) Surface tension calculated from contact angle and Flory–Huggins interaction parameters between donor and acceptors.

the aggregation is evidently promoted with the introduction of CH-D1.

The GIWAXS patterns of neat films and blend films are displayed in Figure 4d–f; and Figure S7 and Table S8 (Supporting Information). All the films reserve a preferential “face on” molecular orientation. As illustrated in Figure 4d–f, the more pronounced diffraction peak of PZC24:CH-D1 film (with the weight ratio of 1:0.3) than PZC24 neat film suggests that the introduction of CH-D1 improves the aggregation, corresponding to the results of AFM images. Figure 4g depicts the (010) d-spacing and crystal coherence length (CCL) in the OOP direction of acceptor films. Note that PZC24:CH-D1 film displays a shorter π – π stacking distance and a larger coherence crystal length (CCL) than PZC24 film, indicating tighter and more ordered molecular packing. These results imply crystallization-induced morphology by CH-D1 can result in better phase connectivity.^[11] When blending with polymer donor PM6, the all-PSCs binary/ternary films exhibit similar (010) scattering peaks located at $\approx 1.66 \text{ \AA}^{-1}$ in the OOP direction. While, the CCL of (010) peak in the OOP direction for the ternary blend is slightly enhanced to 21.49 \AA compared with that of the PM6:PZC24 (Figure 4h). The above results manifest that the introduction of CH-D1 could increase the crystallinity of acceptors, and the corresponding ternary film prefers to form more ordered molecular packing, which guarantees exciton dissociation efficiently as well as facilitate carrier transport as aforementioned before. The tighter molecular packing is benefit for effective charge transfer, so the PM6:CH-D1 film shows the highest PL quenching efficiency excited at 825 nm, followed by that for the ternary film (Figure S5, Supporting Information). Noted that the absorption strength of EQE responses throughout the wavelength of acceptor absorption range is also agreement with these measurements.

To further demonstrate the increased phase-separation in the ternary all-PSCs, the surface energy (γ) values were investigated by measuring the contact angles of the active layer materials using water and glycerol droplets. As shown in Figure 4i, the surface tensions are 18.5 and 20.9 mN m^{-1} for PZC24 and CH-D1, respectively, which is higher than that of donor PM6 (17.4 mN m^{-1}). The Flory–Huggins interaction parameter ($\chi_{D,A}$) is derived from the empirical equation $\chi_{D,A} = \kappa(\sqrt{\gamma_D} - \sqrt{\gamma_A})^2$, where κ is a constant, and γ_D and γ_A are the surface energy of the donor and acceptor films. Among them, PM6:PZC24 shows

the lowest $\chi_{D,A}$ value of 0.017 κ (Figure 4i; and Table S9, Supporting Information), indicating high interfacial compatibility and a low enthalpy of mixing (ΔH_{mix}) between P_D and P_A .^[63] However, CH-D1 shows weaker miscible with whether PM6 or PZC24, demonstrating it can effectively reduce the D:A miscibility, which may be favorable for the higher domain purity and FF in ternary blend film. In addition, we studied the surface energy of blended film of PZC24 and CH-D1 to verify the miscibility for the PM6:PZC24:CH-D1 system. The reckoned χ between PM6 and PZC24:CH-D1 (1:0.3) film is 0.065 κ , which falls in between PM6:PZC24 and PM6:CH-D1 blend films. When comparing two binary systems, the PM6:PZC24 blend has well-mixed domains and thus more D:A interfaces, which are beneficial for exciton dissociation and charge transportation, supporting the higher hole/electron mobilities of PM6:PZC24 blends. However, due to the high compatibility of PM6 and PZC24, it shows slightly more charge recombination, which is evidenced by TPC and TPV results. The introduction of a small amount of CH-D1 not only improves the crystallinity and molecular packing but also maintains the original efficient transport channels of the all-PSCs binary system, leading to the increased J_{SC} and FF simultaneously.

2.5. Mechanical Robustness and Universality

To investigate whether the introduction of dimer acceptor influences the excellent mechanical strength of all-PSCs, the mechanical robustness of neat and blend films were tested by film-on elastomer (FOE) method.^[64,65] Figure S8 (Supporting Information) shows the shape and propagation of cracks when the films were stretched slowly by using FOE method, and relevant results are summarized in Figure 5a. As for the neat films, polymer acceptor shows a crack onset strain (COS) of 6.5%, while dimer acceptor CH-D1 has no mechanical stiffness. Accordingly, PM6:PZC24 all-polymer film possesses larger COS value of $27.3 \pm 0.8\%$ than that of PM6:CH-D1 blend film ($23.1 \pm 2.1\%$). Surprisingly, when introducing CH-D1 to PM6:PZC24 system, the ternary film exhibits slightly enhanced COS of $30.4 \pm 0.8\%$, which can meet the requirement for skin-wearable electronics.^[1] The plasticizing effect of CH-D1 might be responsible for the improved mechanical strength in ternary films. That is, CH-D1 led to stronger π – π stacking and more

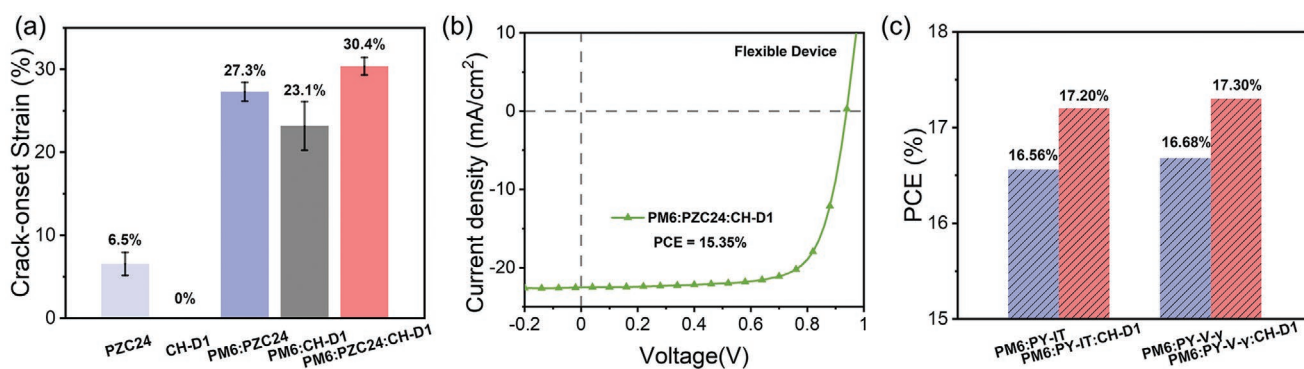


Figure 5. a) Histograms of Crack-onset Strain (COS) measured by the FOE method. b) J – V curves of the flexible cells based on PM6:PZC24:CH-D1. c) Histograms of the PCE of PM6:PY-IT and PM6:PY-V-y systems.

Table 3. Optimized photovoltaic parameters of PM6:PY-IT and PM6:PY-V- γ systems measured under AM 1.5G.

Devices	V_{oc} [V]	J_{sc} [mA cm ⁻²]	J_{sc}^{EQE} [mA cm ⁻²]	FF [%]	PCE [%]
PM6:PY-IT	0.931	23.92	23.83	74.28	16.56
PM6:PY-IT:CH-D1	0.932	24.30	24.00	75.82	17.20
PM6:PY-V- γ	0.899	23.92	23.15	77.21	16.68
PM6:PY-V- γ :CH-D1	0.911	24.87	24.05	76.39	17.30

ordered molecular packing. Through noncovalent interaction between polymers and dimer, the over-aggregation of polymeric conjugate backbones is reduced. In addition, thanks to the similar structure in PZC24 and CH-D1, it shows proper interfacial compatibility between them, which is also beneficial for ductility.^[66–68] With these in mind, we fabricated the ternary flexible cells with the configuration of PEN/ITO/PEDOT:PSS/active layer/F3N/Ag. The J - V curve is displayed in Figure 5b and the detailed photovoltaic parameters are shown in Table 2. The flexible device outputs a PCE of 15.35% with a V_{oc} of 0.939 V, a J_{sc} of 22.53 mA cm⁻² and an FF of 72.60%, which is among the best performance of the reported flexible all-PSCs.

Furthermore, in order to evidence its universality, we introduced CH-D1 to other two classical all-PSC system, PM6:PY-IT and PM6:PY-V- γ , respectively. As depicted in Figure 5c and listed in Table 3, the PCE increases from 16.56% to 17.20% for the former, and from 16.68% to 17.30% for the latter. The obvious enhancement demonstrates that dimer acceptor, CH-D1, is a promising third component in all-PSCs to possess of great superiority in photovoltaic performance.

3. Conclusion

In conclusion, we synthesized a new polymer acceptor PZC24 and its “twins” dimer acceptor CH-D1. Our results revealed that CH-D1 as a third component played an important role in finely increasing the degree of acceptor aggregation and crystallization. As results, the ternary devices displayed more efficient exciton separation, suppressed charge recombination, and enhanced carrier mobility, and thus yielded high FF and J_{sc} values. Consequently, a remarkable PCE of 17.40% is achieved by introducing CH-D1 into the PM6:PZC24 host system, which is obviously higher than those of PM6:PZC24 (16.82%) and PM6:CH-D1 (16.62%) devices. Besides, compared with PM6:PZC24 all-PSCs, the involving of CH-D1 contributed better photo-soaking stability and thermal stability for the all-PSCs devices. Based on the excellent flexibility and stretchability, the ternary flexible photovoltaic cells offered an excellent PCE of 15.35%. Coupled with the excellent universality in other all-PSCs systems, the ternary strategy of introducing oligomer acceptor to all-PSCs not only boosts the PCE and stability, but also can maintain the mechanical robustness of all-PSCs devices, which has the potential to meet the practical needs of wearable electronics.

Supporting Information

Supporting Information is available from the Wiley Online Library or from the author.

Acknowledgements

Z.L. and Z.Z. contributed equally to this work. The authors gratefully acknowledged the financial support from NSFC (Nos. 21935007 and 52025033) and MoST (Nos. 2022YFB4200400 and 2019YFA0705900) of China, Tianjin city (No. 20JCZDJC00740), 111 Project (No. B12015), the 100 Young Academic Leaders Program of Nankai University (No. 020-ZB22000110), the Fundamental Research Funds for the Central Universities, Nankai University (No. 023-ZB22000105), and Haihe Laboratory of Sustainable Chemical Transformations. The authors are grateful for the technical support for Nano-X from Suzhou Institute of Nano-Tech and Nano-Bionics, Chinese Academy of Sciences (SINANNO).

Conflict of Interest

The authors declare no conflict of interest.

Data Availability Statement

The data that support the findings of this study are available from the corresponding author upon reasonable request.

Keywords

all polymer solar cells, dimer acceptors, mechanical flexibility, polymerized small molecular acceptor, ternary devices

Received: January 30, 2023

Revised: February 21, 2023

Published online:

- [1] S. E. Root, S. Savagatrup, A. D. Printz, D. Rodriguez, D. J. Lipomi, *Chem. Rev.* **2017**, *117*, 6467.
- [2] F. Qin, L. Sun, H. Chen, Y. Liu, X. Lu, W. Wang, T. Liu, X. Dong, P. Jiang, Y. Jiang, L. Wang, Y. Zhou, *Adv. Mater.* **2021**, *33*, 2103017.
- [3] Y. Sun, M. Chang, L. Meng, X. Wan, H. Gao, Y. Zhang, K. Zhao, Z. Sun, C. Li, S. Liu, H. Wang, J. Liang, Y. Chen, *Nat. Electron.* **2019**, *2*, 513.
- [4] Y. Huang, C. Jiang, Y. Zhu, S. Zhang, G. Li, Z. Yao, C. Li, X. Wan, Y. Chen, *Org. Electron.* **2022**, *110*, 106642.
- [5] L. Zhan, S. Yin, Y. Li, S. Li, T. Chen, R. Sun, J. Min, G. Zhou, H. Zhu, Y. Chen, J. Fang, C. Q. Ma, X. Xia, X. Lu, H. Qiu, W. Fu, H. Chen, *Adv. Mater.* **2022**, *34*, 2206269.
- [6] Y. Wei, Z. Chen, G. Lu, N. Yu, C. Li, J. Gao, X. Gu, X. Hao, G. Lu, Z. Tang, J. Zhang, Z. Wei, X. Zhang, H. Huang, *Adv. Mater.* **2022**, *34*, 2204718.
- [7] L. Zhan, S. Li, Y. Li, R. Sun, J. Min, Y. Chen, J. Fang, C. Q. Ma, G. Zhou, H. Zhu, L. Zuo, H. Qiu, S. Yin, H. Chen, *Adv. Energy Mater.* **2022**, *12*, 2201076.

- [8] R. Ma, C. Yan, J. Yu, T. Liu, H. Liu, Y. Li, J. Chen, Z. Luo, B. Tang, X. Lu, G. Li, H. Yan, *ACS Energy Lett.* **2022**, *7*, 2547.
- [9] J. Wan, Y. Wu, R. Sun, J. Qiao, X. Hao, J. Min, *Energy Environ. Sci.* **2022**, *15*, 5192.
- [10] C. Han, J. Wang, S. Zhang, L. Chen, F. Bi, J. Wang, C. Yang, P. Wang, Y. Li, X. Bao, *Adv. Mater.* **2023**, *35*, 2208986.
- [11] L. Zhu, M. Zhang, J. Xu, C. Li, J. Yan, G. Zhou, W. Zhong, T. Hao, J. Song, X. Xue, Z. Zhou, R. Zeng, H. Zhu, C. C. Chen, R. C. I. MacKenzie, Y. Zou, J. Nelson, Y. Zhang, Y. Sun, F. Liu, *Nat. Mater.* **2022**, *21*, 656.
- [12] R. Sun, Y. Wu, X. Yang, Y. Gao, Z. Chen, K. Li, J. Qiao, T. Wang, J. Guo, C. Liu, X. Hao, H. Zhu, J. Min, *Adv. Mater.* **2022**, *34*, 2110147.
- [13] Y. Cui, Y. Xu, H. Yao, P. Bi, L. Hong, J. Zhang, Y. Zu, T. Zhang, J. Qin, J. Ren, Z. Chen, C. He, X. Hao, Z. Wei, J. Hou, *Adv. Mater.* **2021**, *33*, 2102420.
- [14] C. He, Y. Pan, Y. Ouyang, Q. Shen, Y. Gao, K. Yan, J. Fang, Y. Chen, C.-Q. Ma, J. Min, C. Zhang, L. Zuo, H. Chen, *Energy Environ. Sci.* **2022**, *15*, 2537.
- [15] D. Li, N. Deng, Y. Fu, C. Guo, B. Zhou, L. Wang, J. Zhou, D. Liu, W. Li, K. Wang, Y. Sun, T. Wang, *Adv. Mater.* **2023**, *35*, 2208211.
- [16] W. Gao, F. Qi, Z. Peng, F. R. Lin, K. Jiang, C. Zhong, W. Kaminsky, Z. Guan, C. S. Lee, T. J. Marks, H. Ade, A. K. Jen, *Adv. Mater.* **2022**, *34*, 2202089.
- [17] P. Bi, J. Wang, Y. Cui, J. Zhang, T. Zhang, Z. Chen, J. Qiao, J. Dai, S. Zhang, X. Hao, Z. Wei, J. Hou, *Adv. Mater.* **2023**, *35*, 2210865.
- [18] K. Chong, X. Xu, H. Meng, J. Xue, L. Yu, W. Ma, Q. Peng, *Adv. Mater.* **2022**, *34*, 2109516.
- [19] J. Gao, N. Yu, Z. Chen, Y. Wei, C. Li, T. Liu, X. Gu, J. Zhang, Z. Wei, Z. Tang, X. Hao, F. Zhang, X. Zhang, H. Huang, *Adv. Sci.* **2022**, *9*, 2203606.
- [20] H. Chen, S. Y. Jeong, J. Tian, Y. Zhang, D. R. Naphade, M. Alsufyani, W. Zhang, S. Griggs, H. Hu, S. Barlow, H. Y. Woo, S. R. Marder, T. D. Anthopoulos, I. McCulloch, Y. Lin, *Energy Environ. Sci.* **2023**, *16*, 1062.
- [21] C. Li, X. Gu, Z. Chen, X. Han, N. Yu, Y. Wei, J. Gao, H. Chen, M. Zhang, A. Wang, J. Zhang, Z. Wei, Q. Peng, Z. Tang, X. Hao, X. Zhang, H. Huang, *J. Am. Chem. Soc.* **2022**, *144*, 14731.
- [22] J. Wang, Y. Cui, Y. Xu, K. Xian, P. Bi, Z. Chen, K. Zhou, L. Ma, T. Zhang, Y. Yang, Y. Zu, H. Yao, X. Hao, L. Ye, J. Hou, *Adv. Mater.* **2022**, *34*, 2205009.
- [23] Y. Wang, H. Yu, X. Wu, D. Zhao, S. Zhang, X. Zou, B. Li, D. Gao, Z. Li, X. Xia, X. Chen, X. Lu, H. Yan, C. C. Chueh, A. K. Y. Jen, Z. Zhu, *Adv. Energy Mater.* **2022**, *12*, 2202729.
- [24] R. Sun, W. Wang, H. Yu, Z. Chen, X. Xia, H. Shen, J. Guo, M. Shi, Y. Zheng, Y. Wu, W. Yang, T. Wang, Q. Wu, Y. Yang, X. Lu, J. Xia, C. J. Brabec, H. Yan, Y. Li, J. Min, *Joule* **2021**, *5*, 1548.
- [25] J. W. Lee, C. Sun, B. S. Ma, H. J. Kim, C. Wang, J. M. Ryu, C. Lim, T. S. Kim, Y. H. Kim, S. K. Kwon, B. J. Kim, *Adv. Energy Mater.* **2020**, *11*, 2003367.
- [26] L. Ma, Y. Cui, J. Zhang, K. Xian, Z. Chen, K. Zhou, T. Zhang, W. Wang, H. Yao, S. Zhang, X. Hao, L. Ye, J. Hou, *Adv. Mater.* **2022**, *35*, 2208926.
- [27] Y. Yue, B. Zheng, W. Yang, L. Huo, J. Wang, L. Jiang, *Adv. Mater.* **2022**, *34*, 2108508.
- [28] Z. Peng, K. Xian, J. Liu, Y. Zhang, X. Sun, W. Zhao, Y. Deng, X. Li, C. Yang, F. Bian, Y. Geng, L. Ye, *Adv. Mater.* **2023**, *35*, 2207884.
- [29] R. Sun, T. Wang, Q. Fan, M. Wu, X. Yang, X. Wu, Y. Yu, X. Xia, F. Cui, J. Wan, X. Lu, X. Hao, A. K. Y. Jen, E. Spiecker, J. Min, *Joule* **2023**, *7*, 7.
- [30] J. Song, Y. Li, Y. Cai, R. Zhang, S. Wang, J. Xin, L. Han, D. Wei, W. Ma, F. Gao, Y. Sun, *Matter* **2022**, *5*, 4047.
- [31] K. Hu, C. Zhu, K. Ding, S. Qin, W. Lai, J. Du, J. Zhang, Z. Wei, X. Li, Z. Zhang, L. Meng, H. Ade, Y. Li, *Energy Environ. Sci.* **2022**, *15*, 4157.
- [32] H. Yu, Y. Wang, H. K. Kim, X. Wu, Y. Li, Z. Yao, M. Pan, X. Zou, J. Zhang, S. Chen, D. Zhao, F. Huang, X. Lu, Z. Zhu, H. Yan, *Adv. Mater.* **2022**, *34*, 2200361.
- [33] D. Zhou, C. Liao, S. Peng, X. Xu, Y. Guo, J. Xia, H. Meng, L. Yu, R. Li, Q. Peng, *Adv. Sci.* **2022**, *9*, 2202022.
- [34] Y. Yue, B. Zheng, J. Ni, W. Yang, L. Huo, J. Wang, L. Jiang, *Adv. Sci.* **2022**, *9*, 2204030.
- [35] Y. Li, Q. Li, Y. Cai, H. Jin, J. Zhang, Z. Tang, C. Zhang, Z. Wei, Y. Sun, *Energy Environ. Sci.* **2022**, *15*, 3854.
- [36] R. Ma, Q. Fan, T. A. Dela Pena, B. Wu, H. Liu, Q. Wu, Q. Wei, J. Wu, X. Lu, M. Li, W. Ma, G. Li, *Adv. Mater.* **2023**, *35*, 2212275.
- [37] T. Zhang, Y. Xu, H. Yao, J. Zhang, P. Bi, Z. Chen, J. Wang, Y. Cui, L. Ma, K. Xian, Z. Li, X.-T. Hao, Z. Wei, J. Hou, *Energy Environ. Sci.* **2023**, <https://doi.org/10.1039/d2ee03535a>.
- [38] G. Wang, F. S. Melkonyan, A. Facchetti, T. J. Marks, *Angew. Chem., Int. Ed.* **2019**, *58*, 4129.
- [39] K. D. Deshmukh, T. Qin, J. K. Gallaher, A. C. Y. Liu, E. Gann, K. O'Donnell, L. Thomsen, J. M. Hodgkiss, S. E. Watkins, C. R. McNeill, *Energy Environ. Sci.* **2015**, *8*, 332.
- [40] Y. Liang, D. Zhang, Z. Wu, T. Jia, L. Lüer, H. Tang, L. Hong, J. Zhang, K. Zhang, C. J. Brabec, N. Li, F. Huang, *Nat. Energy* **2022**, *7*, 1180.
- [41] K. Zhou, K. Xian, L. Ye, *InfoMat* **2022**, *4*, e12270.
- [42] L. Zhang, Z. Zhang, D. Deng, H. Zhou, J. Zhang, Z. Wei, *Adv. Sci.* **2022**, *9*, 2202513.
- [43] Q. Fan, Z. Xiao, E. Wang, L. Ding, *Sci. Bull.* **2021**, *66*, 1950.
- [44] Z. G. Zhang, Y. Yang, J. Yao, L. Xue, S. Chen, X. Li, W. Morrison, C. Yang, Y. Li, *Angew. Chem., Int. Ed.* **2017**, *56*, 13503.
- [45] S. Li, K. Zhou, B. Sun, W. Zhao, L. Ye, *Mater. Today Energy* **2022**, *30*, 101166.
- [46] Q. Li, T. Jia, L.-M. Wang, S. Liu, X. Liao, Z. Cao, J. Zhang, X. Zhan, T. Zhu, Y.-P. Cai, F. Huang, *J. Mater. Chem.* **2022**, *10*, 10880.
- [47] T. Liu, T. Yang, R. Ma, L. Zhan, Z. Luo, G. Zhang, Y. Li, K. Gao, Y. Xiao, J. Yu, X. Zou, H. Sun, M. Zhang, T. A. Dela Peña, Z. Xing, H. Liu, X. Li, G. Li, J. Huang, C. Duan, K. S. Wong, X. Lu, X. Guo, F. Gao, H. Chen, F. Huang, Y. Li, Y. Li, Y. Cao, B. Tang, et al., *Joule* **2021**, *5*, 914.
- [48] Y. Sun, R. Ma, Y. Kan, T. Liu, K. Zhou, P. Liu, J. Fang, Y. Chen, L. Ye, C. Ma, H. Yan, K. Gao, *Macromol. Rapid Commun.* **2022**, *43*, 2200139.
- [49] G. Ding, J. Yuan, F. Jin, Y. Zhang, L. Han, X. Ling, H. Zhao, W. Ma, *Nano Energy* **2017**, *36*, 356.
- [50] S. Li, R. Zhang, M. Zhang, J. Yao, Z. Peng, Q. Chen, C. Zhang, B. Chang, Y. Bai, H. Fu, Y. Ouyang, C. Zhang, J. A. Steele, T. Alshahrani, M. B. J. Roeloffs, E. Solano, L. Meng, F. Gao, Y. Li, Z. G. Zhang, *Adv. Mater.* **2023**, *35*, 2206563.
- [51] H. Wang, C. Cao, H. Chen, H. Lai, C. Ke, Y. Zhu, H. Li, F. He, *Angew. Chem., Int. Ed.* **2022**, *61*, e202201844.
- [52] X. Gu, Y. Wei, N. Yu, J. Qiao, Z. Han, Q. Lin, X. Han, J. Gao, C. Li, J. Zhang, X. Hao, Z. Wei, Z. Tang, Y. Cai, X. Zhang, H. Huang, *CCS Chem.* **2023**, <https://doi.org/10.31635/ccschem.023.202202575>.
- [53] W. Liu, J. Yuan, C. Zhu, Q. Wei, S. Liang, H. Zhang, G. Zheng, Y. Hu, L. Meng, F. Gao, Y. Li, Y. Zou, *Sci. China Chem.* **2022**, *65*, 1374.
- [54] Y. Zou, H. Chen, X. Bi, X. Xu, H. Wang, M. Lin, Z. Ma, M. Zhang, C. Li, X. Wan, G. Long, Y. Zhaoyang, Y. Chen, *Energy Environ. Sci.* **2022**, *15*, 3519.
- [55] H. Chen, Y. Zou, H. Liang, T. He, X. Xu, Y. Zhang, Z. Ma, J. Wang, M. Zhang, Q. Li, C. Li, G. Long, X. Wan, Z. Yao, Y. Chen, *Sci. China Chem.* **2022**, *65*, 1362.
- [56] H. Chen, H. Liang, Z. Guo, Y. Zhu, Z. Zhang, Z. Li, X. Cao, H. Wang, W. Feng, Y. Zou, L. Meng, X. Xu, B. Kan, C. Li, Z. Yao, X. Wan, Z. Ma, Y. Chen, *Angew. Chem., Int. Ed.* **2022**, *61*, e202209580.
- [57] X. Li, Q. Zhang, J. Yu, Y. Xu, R. Zhang, C. Wang, H. Zhang, S. Fabiano, X. Liu, J. Hou, F. Gao, M. Fahlman, *Nat. Commun.* **2022**, *13*, 2046.

- [58] S. Vishal, Y. Yao, G. Li, Y. Yang, *Appl. Phys. Lett.* **2006**, *89*, 063505.
- [59] J. Wu, F. Chen, Y. Hsiao, M. H. Huang, C. Hsu, *ACS Nano* **2011**, *5*, 959.
- [60] Z. Wang, K. Gao, Y. Kan, M. Zhang, C. Qiu, L. Zhu, Z. Zhao, X. Peng, W. Feng, Z. Qian, X. Gu, A. K. Jen, B. Z. Tang, Y. Cao, Y. Zhang, F. Liu, *Nat. Commun.* **2021**, *12*, 332.
- [61] F. Huang, Z. Li, G. Song, C. Jiang, Y. Yang, J. Wang, X. Wan, C. Li, Z. Yao, Y. Chen, *Adv. Funct. Mater.* **2023**, *33*, 2211140.
- [62] S. Liu, J. Yuan, W. Deng, M. Luo, Y. Xie, Q. Liang, Y. Zou, Z. He, H. Wu, Y. Cao, *Nat. Photonics* **2020**, *14*, 300.
- [63] L. Ma, S. Zhang, J. Ren, G. Wang, J. Li, Z. Chen, H. Yao, J. Hou, *Angew. Chem., Int. Ed.* **2023**, *62*, e202214088.
- [64] Z. Peng, K. Xian, Y. Cui, Q. Qi, J. Liu, Y. Xu, Y. Chai, C. Yang, J. Hou, Y. Geng, L. Ye, *Adv. Mater.* **2021**, *33*, 2106732.
- [65] B. Zhao, D. Pei, Y. Jiang, Z. Wang, C. An, Y. Deng, Z. Ma, Y. Han, Y. Geng, *Macromolecules* **2021**, *54*, 9896.
- [66] J. Mun, J. Kang, Y. Zheng, S. Luo, H. C. Wu, N. Matsuhisa, J. Xu, G. N. Wang, Y. Yun, G. Xue, J. B. Tok, Z. Bao, *Adv. Mater.* **2019**, *31*, 1903912.
- [67] J. Xu, H. C. Wu, J. Mun, R. Ning, W. Wang, G. N. Wang, S. Nikzad, H. Yan, X. Gu, S. Luo, D. Zhou, J. B. Tok, Z. Bao, *Adv. Mater.* **2022**, *34*, 2104747.
- [68] J. Mun, J. Kang, Y. Zheng, S. Luo, Y. Wu, H. Gong, J. C. Lai, H. C. Wu, G. Xue, J. B. H. Tok, Z. Bao, *Adv. Electron. Mater.* **2020**, *6*, 2000251.